

# Cosmological bounds on sub-MeV mass axions

Davide Cadamuro<sup>a</sup> Steen Hannestad<sup>b</sup> Georg Raffelt<sup>a</sup>  
Javier Redondo<sup>a</sup>

<sup>a</sup>Max-Planck-Institut für Physik (Werner-Heisenberg-Institut)  
Föhringer Ring 6, D-80805 München, Germany

<sup>b</sup>Department of Physics and Astronomy  
University of Aarhus, DK-8000 Aarhus C, Denmark

E-mail: [cadamuro@mppmu.mpg.de](mailto:cadamuro@mppmu.mpg.de), [sth@phys.au.dk](mailto:sth@phys.au.dk), [raffelt@mppmu.mpg.de](mailto:raffelt@mppmu.mpg.de),  
[redondo@mppmu.mpg.de](mailto:redondo@mppmu.mpg.de)

**Abstract.** Axions with mass  $m_a \gtrsim 0.7$  eV are excluded by cosmological precision data because they provide too much hot dark matter. While for  $m_a \gtrsim 20$  eV the  $a \rightarrow 2\gamma$  lifetime drops below the age of the universe, we show that the cosmological exclusion range can be extended to  $0.7 \text{ eV} \lesssim m_a \lesssim 300 \text{ keV}$ , primarily by the cosmic deuterium abundance: axion decays would strongly modify the baryon-to-photon ratio at BBN relative to the one at CMB decoupling. Additional arguments include neutrino dilution relative to photons by axion decays and spectral CMB distortions. Our new cosmological constraints complement stellar-evolution and laboratory bounds.

---

## Contents

<b>1</b>	<b>Introduction</b>	<b>1</b>
<b>2</b>	<b>Axion properties</b>	<b>2</b>
<b>3</b>	<b>Decaying axion cosmology</b>	<b>3</b>
3.1	Primakoff decoupling and axion abundance	5
3.2	Entropy production by axion decay	6
<b>4</b>	<b>Big-bang nucleosynthesis</b>	<b>7</b>
<b>5</b>	<b>Neutrino dilution</b>	<b>9</b>
5.1	Radiation density at CMB decoupling	9
5.2	Axion bounds	11
<b>6</b>	<b>CMB distortions</b>	<b>12</b>
<b>7</b>	<b>Conclusions</b>	<b>13</b>
<b>A</b>	<b>Axion out-of-equilibrium decay</b>	<b>14</b>
A.1	Boltzmann equation	14
A.2	Axion decay	16

---

## 1 Introduction

The era of precision cosmology has opened new opportunities to use the universe as a particle-physics laboratory. Cosmological neutrino mass limits and the prospect of eventually measuring this fundamental parameter in the sky is, of course, the most notable example [1, 2]. Analogous arguments allow to derive limits on other hypothetical low-mass particles and here axions are perhaps the most interesting case [3–7], where cosmological data imply  $m_a < 0.7$  eV [8]. Of course, if axions are the cold dark matter of the universe [9], they are very light ( $m_a \lesssim 10$   $\mu$ eV) and such arguments are moot. Therefore, the hot dark matter limits are primarily useful to complement stellar energy-loss arguments [10] and the direct search for solar axions by CAST at CERN [11] and the Tokyo axion helioscope [12].

Axions decay by  $a \rightarrow 2\gamma$ , the lifetime dropping below the age of the universe for  $m_a \gtrsim 20$  eV. For a sufficiently large mass, the decay happens early enough to thermalize the secondary photons and hot-dark matter or overclosure arguments no longer apply.

However, decaying axions are still constrained by several cosmological arguments. Before the cosmological precision era, such questions were discussed in great detail for axion-like particles [13, 14]. A central argument was the impact of excess radiation provided by axions during big-bang nucleosynthesis (BBN). Today it has become clear that BBN does not credibly exclude excess radiation provided by one additional thermal degree of freedom and some amount of excess radiation may even be favoured [15, 16]. Moreover, cosmological precision data somewhat prefer excess radiation equivalent to 1–2 neutrino species at the epoch of CMB decoupling [17–21]. Therefore, we here address the question which axion mass range beyond 0.7 eV is actually excluded by cosmological arguments alone.

If axions decay not too early, spectral distortions of the CMB provide restrictive constraints [14]. For earlier decays (larger masses), the decay photons thermalize and heat the CMB relative to cosmic neutrinos. Since all cosmological quantities are normalized to the *measured* CMB temperature, this means that effectively neutrinos are diluted. If axions decay non-relativistically and thus out of equilibrium, this effect can be large and leads to a lowered radiation density at CMB decoupling, increasing the tension with precision data that actually favour a radiation excess. Most importantly, the baryon density at CMB decoupling is also diluted. Therefore, the baryon abundance relevant for BBN is larger than implied by CMB data, leading to a smaller primordial deuterium abundance. Confronting this with observations requires that axions are not significantly abundant during BBN. This new BBN limit requires  $m_a \gtrsim 300$  keV. Our new bounds therefore nicely overlap with the constraints from beam dump and reactor experiments [22–27].

To derive this result we first describe the relevant phenomenological properties of axions in Sec. 2. In Sec. 3, we discuss the modification of the cosmic expansion history and the relative contributions of different forms of radiation in our decaying axion scenario. Constraints based on BBN, neutrino dilution, and CMB distortions are presented in Secs. 4–6 before concluding in Sec. 7.

## 2 Axion properties

The axion arises in the Peccei-Quinn solution of the strong CP problem as the Nambu-Goldstone boson of a new global spontaneously broken  $U(1)_{\text{PQ}}$  axial symmetry [28]. The main ingredient of the PQ mechanism is that  $U(1)_{\text{PQ}}$  is colour anomalous, providing for an axion-gluon interaction of the form

$$\mathcal{L}_{aGG} = \frac{a}{f_a} \frac{\alpha_s}{8\pi} G_a^{\mu\nu} \tilde{G}_{a\mu\nu}. \quad (2.1)$$

The energy scale  $f_a$ , the axion decay constant, is the main parameter that fixes low-energy axion phenomenology. This term automatically cancels the CP-violating  $\theta$  term of QCD because it generates nonperturbatively a potential for the axion, driving the axion field to the CP-conserving position. The axion mass thus created is

$$m_a = \frac{f_\pi m_\pi}{f_a} \frac{\sqrt{z}}{1+z} \simeq 6 \text{ eV} \left( \frac{10^6 \text{ GeV}}{f_a} \right), \quad (2.2)$$

where  $m_\pi = 135$  MeV is the neutral pion mass,  $f_\pi = 92$  MeV its decay constant, and  $z = m_u/m_d$ . We use the canonical value  $z = 0.56$ , although the possible range is  $z = 0.35$ – $0.6$  [29], implying a 10% uncertainty of the axion mass.

In the minimal scenario we shall consider, axions do not have tree-level interactions with leptons. There are thus called *hadronic* axions. The freeze-out of sub-eV hadronic axions is determined by their interaction with pions. However, we here consider much larger masses and much later freeze-out. Their only relevant interaction is with photons,

$$\mathcal{L}_{a\gamma\gamma} = \frac{g_{a\gamma}}{4} F^{\mu\nu} \tilde{F}_{\mu\nu} a = -g_{a\gamma} \mathbf{E} \cdot \mathbf{B} a, \quad (2.3)$$

where  $F$  is the electromagnetic field-strength tensor,  $\tilde{F}$  its dual, and  $\mathbf{E}$  and  $\mathbf{B}$  the electric and magnetic field, respectively. The coupling constant

$$g_{a\gamma} = \frac{\alpha}{2\pi f_a} \left( \frac{E}{N} - \frac{24+z}{31+z} \right) \equiv \frac{\alpha}{2\pi f_a} 1.9 \delta, \quad (2.4)$$

consists of a model-independent contribution from  $a$ - $\pi$ - $\eta$  mixing and a model-dependent one parameterized by the ratio  $E/N$  of the  $U(1)_{\text{PQ}}$  electromagnetic and colour anomalies. The uncertainties from the up/down quark-mass ratio  $z$  and from the model-dependence of  $E/N$  can be lumped into the parameter  $\delta$ . We have normalized  $\delta$  such that  $\delta = 1$  for  $E = 0$ , happening for instance in the KSVZ model [30, 31].

The well-known  $a \rightarrow 2\gamma$  decay rate is

$$\Gamma_{a \rightarrow \gamma\gamma} = \frac{g_{a\gamma}^2 m_a^3}{64\pi} \simeq 1.1 \times 10^{-24} \text{ s}^{-1} \left( \frac{m_a}{\text{eV}} \right)^5 \delta^2. \quad (2.5)$$

For  $\delta = 1$ , axions with  $m_a < 18$  eV live longer than the age of the universe. In this paper, we shall consider  $\delta$  values of order one, excluding radical fine-tuning or very large  $E/N$  scenarios. Note however, that a value  $\delta = 0$  provides the most restrictive limit: axions would not disappear and eventually over-close the universe.

In extended models such as the DFSZ [32, 33], axions also have tree-level interactions with leptons. The Nambu-Goldstone boson nature of axions determines the form of the interaction to be of the derivative axial-current form [34]

$$\mathcal{L}_l = \frac{C_l}{2f_a} \bar{\psi}_l \gamma^\mu \gamma_5 \psi_l (\partial_\mu a) \equiv \frac{C_l m_l}{f_a} \bar{\psi}_l \gamma_5 \psi_l a, \quad (2.6)$$

where the  $C_l$ 's are model-dependent numerical coefficients. Note that the coupling is proportional to the lepton mass<sup>1</sup>. For late cosmology we will be mostly interested in the coupling to electrons since the coupling to neutrinos is extremely suppressed by the small neutrino masses.

### 3 Decaying axion cosmology

Our main cosmological arguments depend on modified baryon-to-photon and neutrino-to-photon ratios at various epochs. One difficulty is that the freeze-out epoch of axions in the relevant mass range can coincide with the  $e^+e^-$  annihilation epoch and with the BBN epoch itself. Moreover, for  $m_a \lesssim 20$  keV, axions first decouple from the Primakoff process and then recouple by inverse decays, causing a somewhat complicated evolution of the radiation fields. As a first step we therefore discuss this evolution.

Thermal axions are produced after the QCD epoch by hadronic processes such as  $\pi + \pi \leftrightarrow \pi + a$ . As the universe cools, hadrons disappear and the photo-production of axions from electrons,  $e^\pm \gamma \rightarrow e^\pm a$ , dominate. For hadronic axions, the most relevant reaction is the Primakoff process (see Fig. 8a in Appendix A). A simple estimate for  $T \gg m_a$  is

$$\Gamma_P \sim \alpha g_{a\gamma}^2 n_e, \quad (3.1)$$

where  $n_e$  is the density of electrons plus positrons. For non purely hadronic axions, the direct axion-electron coupling allows for the Compton process (see Fig. 8b in Appendix A). An estimate of its rate is

$$\Gamma_C \sim \alpha \frac{g_{ae}^2}{\max\{T^2, m_e^2\}} n_e. \quad (3.2)$$

---

<sup>1</sup>The equivalence between the axial and pseudoscalar forms of Eq. (2.6) is not always guaranteed but it will be so for the applications of this paper where we consider processes involving the emission or absorption of one Nambu-Goldstone boson at a time.

At temperatures close to the electron mass, this process is more efficient than the Primakoff since involves less powers of  $\alpha$ , and when present will dominate the axion thermalization. Other processes like  $e^+e^- \rightarrow \gamma a$  are subdominant and can be neglected in the following. More details about the Primakoff and Compton processes are given in Appendix A.

The Primakoff and/or Compton processes freezes out when their rate drops below the cosmic expansion rate

$$H = \frac{1}{R} \frac{dR}{dt} = \sqrt{\frac{8\pi}{3m_{\text{Pl}}^2} \rho} \equiv \sqrt{\frac{8\pi}{3m_{\text{Pl}}^2} \frac{\pi^2}{30} g_*} T^2, \quad (3.3)$$

where  $R$  is the cosmic scale factor,  $m_{\text{Pl}} = 1.22 \times 10^{19}$  GeV is the Planck mass,  $\rho$  the total energy density of the universe,  $T$  the photon temperature and the last equality defines  $g_*$ , the effective number of thermally excited degrees of freedom. The rates  $\Gamma_P$  and  $\Gamma_C$  decrease exponentially when  $e^+e^-$  annihilation sets in, so the Primakoff and Compton processes indeed freeze out (see Fig. 1).

Another processes based on the two-photon vertex are decay and inverse decay. For  $T \gg m_a$  the inverse decay rate is

$$\Gamma_{\gamma\gamma \rightarrow a} \simeq \Gamma_{a \rightarrow \gamma\gamma} \frac{m_a^2 - 4m_\gamma^2}{m_a^2} \left\langle \frac{m_a}{\omega} \right\rangle, \quad (3.4)$$

where  $\langle m_a/\omega \rangle$  is a thermally averaged time dilatation factor. Decay or inverse decay is only possible if  $m_a > 2m_\gamma$ , where  $m_\gamma$  is the plasmon mass. For  $T \gg m_e$ , we have  $m_\gamma = \sqrt{3\alpha\pi/2} T \lesssim T$  while for  $T \ll m_e$  we have  $m_\gamma \ll T$  so the decay/inverse decay channels open up not far from  $m_a \sim \max\{T, m_e\}$ . Leaving aside the threshold, for relativistic axions  $\Gamma_{\gamma\gamma \rightarrow a} \propto T^{-1}$  and this process actually recouples at a certain temperature (thin solid line in Fig. 1).

In Fig. 1 we show the decoupling and recoupling temperatures (horizontal axis) as a function of axion mass (vertical axis). For a given  $m_a$  the cooling universe moves on a horizontal line from right to left, beginning with axions in thermal equilibrium (yellow shaded). For  $m_a \gtrsim 20$  keV the horizontal line never leaves yellow territory and axions remain in thermal equilibrium forever, first by the Primakoff process and later by inverse decays. If axions couple to electrons, this region is extended until  $m_a \sim 10$  keV through the Compton process. In this case, the cosmic axion history is governed by thermal equilibrium. The populations of all forms of radiation are determined by entropy conservation (adiabatic regime).

Another relatively simple range is  $m_a \lesssim 1$  keV where Primakoff freezes out when the  $e^+e^-$  plasma is fully populated and Compton is not very effective. The approximate temperature range of  $e^+e^-$  annihilation is delimited by the two thin vertical lines in Fig. 1. In this mass range recoupling occurs for  $T \ll m_a$  as we can see in Fig. 1 where the diagonal dashed line denotes  $T = 3m_a$ . Notice that here recoupling means axion decay since the putative thermal axion population is exponentially Boltzmann suppressed. Entropy is generally produced in the recoupling process, which in this case can be quite sizeable. In the approximate  $m_a$  range 1–5 keV, axions decouple during the  $e^+e^-$  annihilation epoch, but once more recouple in the Boltzmann suppressed regime. For  $m_a = 5$ –20 keV axions recouple under relativistic conditions.

For axion-photon interaction strength  $\delta \neq 1$  the overall behaviour is similar. Both the Primakoff and decay rates are proportional to  $\delta^2$  and are increasing functions of  $m_a$ . Therefore, a value  $\delta < 1$  can be compensated by a increase in  $m_a$  and vice versa, so the

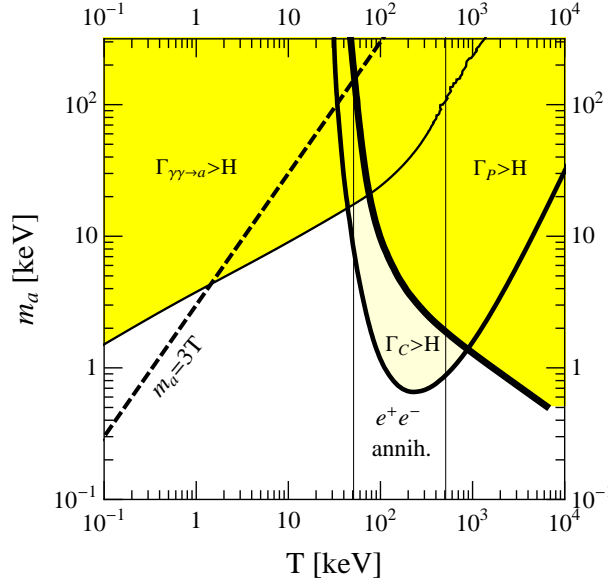


**Figure 1.** Axion decoupling and recoupling ( $\delta = 1$ ,  $C_e = 1/6$ ). Thick solid line: Freeze-out of Primakoff process. Medium solid line: Coupling and freeze-out of the Compton process. Thin solid line: Recoupling of inverse decay. In the yellow shaded region, axions are in thermal equilibrium, where the lighter yellow region is only relevant if the Compton process is effective. The dashed diagonal line denotes  $m_a = 3T$ . The vertical lines delimit the  $e^+e^-$  annihilation epoch.

decoupling and recoupling curves move upwards when  $\delta < 1$  and downwards for  $\delta > 1$ . The same holds for the coupling to electrons  $C_e$  which we have taken to be  $1/6$  in Fig. 1.

### 3.1 Primakoff decoupling and axion abundance

Next we must find the axion population existing after Primakoff/Compton decoupling in those cases when axions actually leave thermal equilibrium, i.e. when the cosmic evolution in Fig. 1 cuts through white space. We must solve the Boltzmann collision equation for the evolution of the axion number density  $n_a$  during the  $e^+e^-$  annihilation epoch. We cast the Boltzmann equation in the form

$$\frac{dY_a}{d \log T} = \frac{\Gamma_e + \Gamma_{\gamma\gamma \rightarrow a}}{H} \frac{d \log s}{d \log T^3} (Y_a - Y_a^{\text{eq}}) , \quad (3.5)$$

where  $Y_a = n_a/s$  and  $s$  is the entropy density. We have numerically solved for the evolution of  $Y_a$  and show the final axion abundance after  $e^+e^-$  annihilation in Fig. 2. Hadronic axions with  $m_a \gtrsim 20$  keV indeed keep thermal abundance. For smaller  $m_a$ , the final abundance is smaller because axions decouple before the  $e^+e^-$  entropy is fully released: they end up colder than photons (which define the equilibrium temperature). If axions couple to electrons the situation is very much the same except that the Compton process being more effective the abundances are generally larger than in the purely hadronic case.

Axions modify the photon abundance in crucial ways whereas neutrinos are unaffected. Therefore, it proves convenient to normalize abundances in terms of the neutrino temperature which redshifts as  $T_\nu \propto R^{-1}$  after the neutrino decoupling. So we parameterize the axion

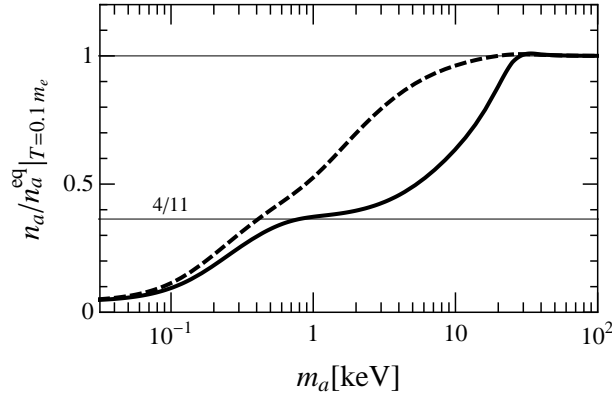


**Figure 2.** Axion number density  $n_a$  after  $e^+e^-$  annihilation from numerically solving the Boltzmann equation until  $T = m_e/10$ . The equilibrium density  $n_a^{\text{eq}}$  is defined in terms of the photon temperature. Solid line: only Primakoff process (hadronic axions). Dashed line: Primakoff and Compton.

and photon abundances in terms of their temperatures as

$$A = \left(\frac{T_a}{T_\nu}\right)^3 \quad \text{and} \quad B = \left(\frac{T}{T_\nu}\right)^3. \quad (3.6)$$

As initial condition we use  $T_0 = T_{\nu,0} = T_{a,0} = 2$  MeV when neutrinos have decoupled and  $e^+e^-$  annihilation has not yet begun. The final epoch is defined by  $T_1 = m_e/10$ . Entropy conservation during  $e^+e^-$  annihilation implies

$$\frac{7}{2} + 2 + A_0 = 2B_1 + A_1, \quad (3.7)$$

where  $7/2$  and  $2$  are the  $e^+e^-$  and  $\gamma$  entropy degrees of freedom. From Fig. 1 we see that all of this happens far below the dashed line, i.e. axions are relativistic. We assume kinetic equilibrium even if axions decouple during the  $e^+e^-$  annihilation.

If axions decouple before  $e^+e^-$  annihilation like neutrinos we have  $A_1 = A_0$ . They do not receive any  $e^+e^-$  entropy and photons are heated by the standard amount, i.e.  $B_1 = \frac{11}{4}$ .

On the other hand, if axions decouple during or after  $e^+e^-$  annihilation they are somewhat heated. We always have  $A_0 = 1$  and thus

$$B_1 = \frac{13}{2(h_1 + 2)} \quad \text{where} \quad h = \frac{A}{B} = \left(\frac{T_a}{T}\right)^3 = \frac{n_a}{n_a^{\text{eq}}} = \frac{s_a}{s_a^{\text{eq}}}. \quad (3.8)$$

It is  $h$  that was plotted in Fig. 2. If axions are fully coupled during  $e^+e^-$  annihilation, then  $h_1 = 1$  and  $B_1 = \frac{13}{6}$ . In general we will have  $\frac{11}{4} < B_1 < \frac{13}{6}$ .

### 3.2 Entropy production by axion decay

Eventually axions disappear and transfer their entropy to the photon bath, increasing the photon density both relative to neutrinos and baryons. If axions never leave thermal equilibrium (for  $m_a \gtrsim 20$  keV), we easily find that the final photon abundance is  $\frac{13}{11}$  times the standard value. In general the entropy transfer to photons depends on two parameters, the initial axion abundance, parameterized by  $h$ , and the effectiveness of inverse decay when

axions become non-relativistic. To determine the final photon abundance we have solved numerically for the axion phase-space evolution (Appendix A). Here we only highlight the extreme cases of adiabatic decay (happening when inverse decay is effective at the time axions become non-relativistic) and out-of-equilibrium decay (when the inverse decay is ineffective).

If axions recouple relativistically, their temperature must catch up with photons and the latter are cooled. In this process, radiation is simply shuffled from one form to another and co-moving energy remains conserved. After axion recoupling, the photon abundance is reduced to  $B_* = B_1 [(2 + h_1^{4/3})/(2 + 1)]^{3/4}$ . Comoving entropy increases by the factor  $[(2 + 1)/(2 + h_1)]B_*/B_1$ , but this is never a big effect. For  $h_1 = 4/11$  the entropy increases by some 2.6%. Later when axions get Boltzmann suppressed, this adiabatic process transfers their entropy to the photon bath, heating it according to  $B_2/B_* = (2+1)/2 = 3/2$ . Therefore, the final photon heating by axion recoupling and adiabatic decay is given by

$$\frac{B_2}{B_1} = \frac{3}{2} \left( \frac{2 + h_1^{4/3}}{3} \right)^{3/4}. \quad (3.9)$$

This ratio is the number density of photons relevant at CMB decoupling relative to the density they would have without axion effects, where in both cases the density is measured relative to neutrinos. Without axions  $B_2/B_1 = 1$ .

If axions recouple non-relativistically, their out-of-equilibrium decay can produce a large amount of entropy. This point is illustrated by an analytic approximation to the entropy generation [35]

$$\frac{B_2}{B_1} = 1.83 \langle g_{*S}^{1/3} \rangle^{3/4} \frac{m_a Y_a(T_1)}{\sqrt{m_{\text{Pl}} \Gamma_{a \rightarrow \gamma\gamma}}} = 2.8 \times 10^3 \frac{h_1}{\delta} \left( \frac{500 \text{ eV}}{m_a} \right)^{3/2}, \quad (3.10)$$

where  $g_{*S}$  is the effective number of entropy degrees of freedom and  $\langle g_{*S}^{1/3} \rangle$  denotes an average over the decay time. In the last equality we have taken  $g_{*S} = g_{*S}(T_1) = 3.9$ .

For our actual BBN and neutrino dilution arguments in the following sections we have numerically calculated the photon heating relative to neutrinos as a function of  $m_a$  by solving the Boltzmann equation (Appendix A). In Fig. 3 we show the resulting  $B_2/B_1$  as a function of  $m_a$  in the case  $\delta = 1$ .

## 4 Big-bang nucleosynthesis

The outcome of standard BBN depends basically on the parameter  $\eta = n_B/n_\gamma$ , the baryon-to-photon ratio. The overall agreement of the predicted light-element abundances with observations implies  $5.1 < \eta_{10} < 6.5$  at 95% C.L. [29], where  $\eta_{10} = 10^{10}\eta$ . An independent determination  $\eta_{10} = 6.23 \pm 0.17$  derives from the CMB temperature fluctuations [19]. The concordance between the BBN and CMB implied values will be disturbed in the decaying axion cosmology because the baryon abundance is diluted after BBN. In our scenario  $\eta^{\text{BBN}}/\eta^{\text{CMB}} = B_2/B_1$  and therefore it follows the same curve depicted in Fig. (3). An increased baryon abundance relative to photons during BBN implies that nuclear reactions are more efficient, the deuterium bottleneck opens earlier, decreasing the residual deuterium abundance and increasing the yield of heavier elements. The increased expansion rate caused by the presence of axions works in the opposite direction but plays a sub-leading role.

In order to quantify our arguments we have modified the publicly available BBN code `ParthENoPE` [36] to include the effects of axions, taking into account their impact on the



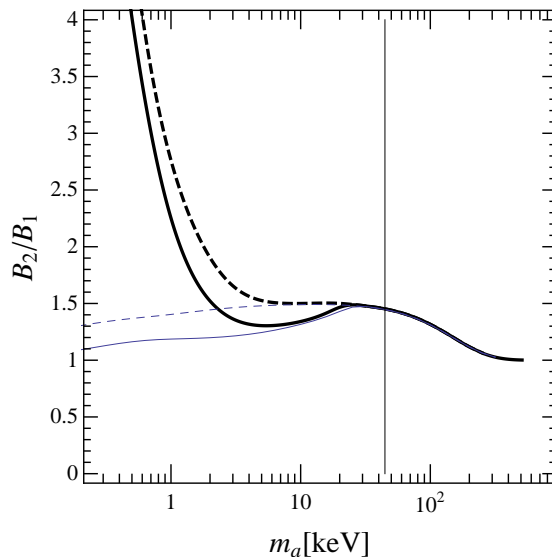


**Figure 3.** Photon density increase in our modified cosmology as expressed by  $B_2/B_1$  for  $\delta = 1$ . Solid and dashed lines stand for hadronic and non-hadronic ( $C_e = 1/6$ ) axions respectively. The thin lines show the value if we assume that no entropy is generated in axion decay.

Friedmann equation and the modified densities of different radiation species. Our results are shown in Fig. 4. For  $m_a > 20$  keV we treat axions as being in thermal equilibrium throughout BBN. For  $m_a \lesssim 10$  keV we use their abundance from our numerical freeze-out calculation, assuming that they are decoupled during BBN. We do not treat the intermediate case, leaving a gap in the predicted deuterium yield as a function of  $m_a$  that is shown as a red band in Fig. 4. To calculate this curve we have adjusted the baryon abundance such that in the very end it matches the CMB-implied value. Its  $1\sigma$  range is represented by the width of the red band.

We compare the predicted D yield with the measured value  $D/H|_p = (2.82 \pm 0.21) \times 10^{-5}$  [29], estimated from 7 high-redshift, low-metallicity clouds absorbing the light of background quasars [37]. The dark (light) grey band in Fig. 4 is the experimental 95% (99%) C.L. region. We have included the independent determination of  $D/H|_p$  from the 7 systems in the right panel of Fig. 4 as function of the H column density. Note that there is a significant scatter of the results whose origin still remains unclear and that has been taken into account by artificially increasing the error (the width of the grey band) [37]. Such a large scatter in the measurements of the D abundance may be a signal of some not yet understood processing of D inside these high-redshift clouds. Whether this is the case or not, there are no known astration processes that increase the D concentration, so the primordial  $y_D$  should be *larger* than this estimation. As we see in Fig. 4, the presence of axions reduces  $y_D$ , so our bounds appear to be conservative regarding this possible systematic.

The deuterium abundance is reduced below its  $2\sigma$  observation if  $m_a$  is below 300 keV. Therefore, BBN constrains axions to have masses

$$m_a > 300 \text{ keV} . \quad (4.1)$$

Axions with mass above this limit have almost completely disappeared from the thermal bath before they can affect BBN and the predictions approach standard BBN. Since this bound

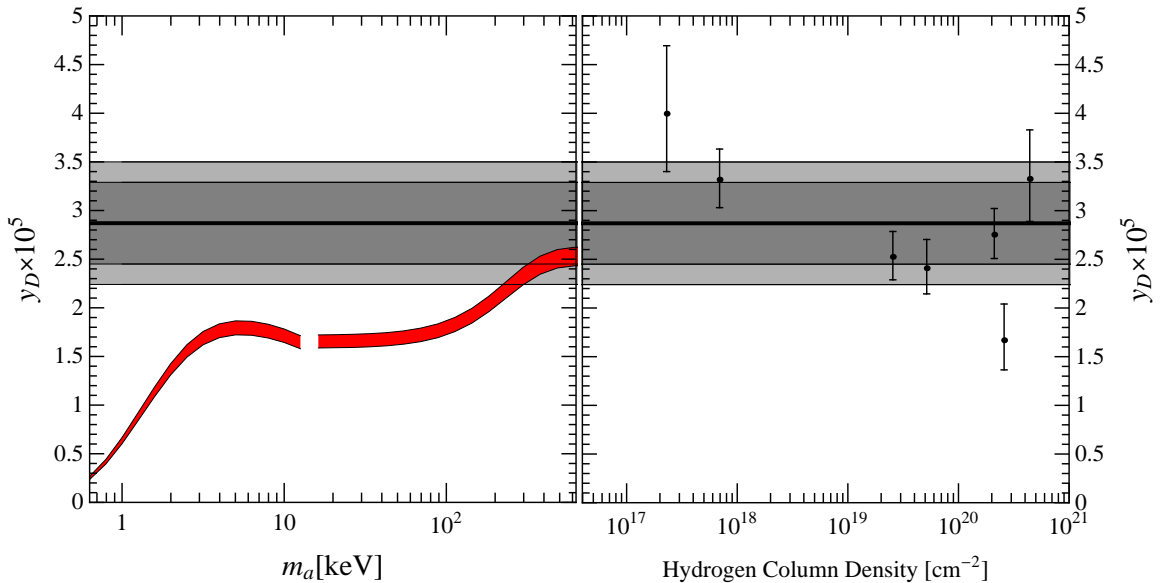


**Figure 4.** Deuterium yield  $y_D$  as a function of  $m_a$  for  $\delta = 1$  (Hadronic axions). The width of the red band represents the  $1\sigma$  uncertainty of the CMB determination of  $\eta$ . To the right of the break, axions are treated as being in LTE, to the left they are assumed to be decoupled during BBN. The grey bands represent the 95% and 99% range for the observed D abundance. It is derived from 7 high redshift Ly- $\alpha$  clouds with individual results shown in the right panel as a function of the hydrogen column density [37].

corresponds to axions that are always in thermal equilibrium, even only via the Primakoff and inverse decay processes, it also applies to non-hadronic axions which would interact more strongly. Note finally that the helium yield is only mildly affected and does not provide interesting bounds.

## 5 Neutrino dilution

### 5.1 Radiation density at CMB decoupling

We have seen that thermally excited axions that eventually disappear increase the abundance of photons at CMB decoupling relative to baryons and neutrinos. Since all cosmic parameters are defined relative to the observed CMB properties, this means that effectively the neutrino abundance is reduced. The impact of this effect on the CMB determination of the cosmic baryon abundance is minimal and thus could be neglected in the previous section. However, precision observables also measure the cosmic radiation density at decoupling, and here the “missing neutrinos” should make a difference.

To extract cosmological information on the radiation density at CMB decoupling we analyse the usual 8-parameter standard  $\Lambda$ CDM model described in Ref. [8], extended in two ways. We allow the effective number of neutrino degrees of freedom to vary, assuming a flat prior on the interval  $0 < N_{\text{eff}} < 3.0$ . We recall that the radiation energy density is

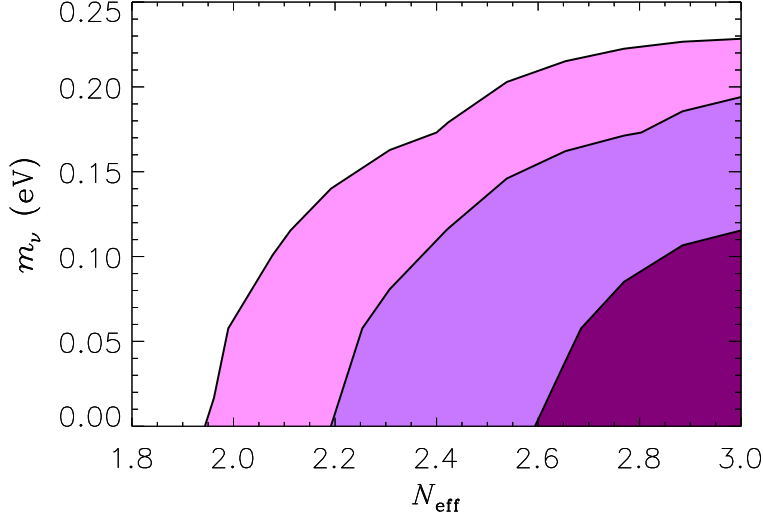


**Figure 5.** 2D marginal 68%, 95% and 99% contours in the  $m_\nu$ – $N_{\text{eff}}$  plane, where  $m_\nu$  is the individual neutrino mass (not the often-used sum over masses).

traditionally expressed as

$$\rho_{\text{rad}} = \left[ 1 + \frac{7}{8} \left( \frac{4}{11} \right)^{4/3} N_{\text{eff}} \right] \rho_\gamma, \quad (5.1)$$

where the photon radiation density is  $\rho_\gamma = (\pi^2/15)T^4$  and  $N_{\text{eff}}$  the effective number of thermally excited neutrino degrees of freedom. The standard value is  $N_{\text{eff}} = 3.046$  instead of 3 because of residual neutrino heating by  $e^+e^-$  annihilation [38] but, given the current experimental uncertainty, we neglect this tiny correction. In addition, we allow for neutrino masses, assuming a common value  $m_\nu$  for all flavours and a flat prior on  $0 < \Omega_\nu/\Omega_m < 1$ . The other parameters and their priors are identical with those provided in Ref. [8]. Moreover, we use the same set of cosmological data, i.e., the WMAP 7-year CMB measurements, the 7th data release of the Sloan Digital Sky Survey, and the Hubble constant from Hubble Space Telescope observations.

Marginalizing over all parameters but  $m_\nu$  and  $N_{\text{eff}}$  we find the 2D credible regions shown in Fig. 5. Marginalizing in addition over  $m_\nu$  we find the limits

$$N_{\text{eff}} > \begin{cases} 2.70 & \text{at 68\% C.L.} \\ 2.39 & \text{at 95\% C.L.} \\ 2.11 & \text{at 99\% C.L.} \end{cases} \quad (5.2)$$

These limits are very restrictive because on present evidence cosmology actually prefers extra radiation beyond  $N_{\text{eff}} > 3$  [17–21]. Taking this possibility seriously, we would need to worry about *two* novel ingredients: axions and radiation in some new form.

The PLANCK satellite, currently taking CMB data, is expected to boost precision determinations of cosmological parameters. It will measure the cosmic radiation content at CMB decoupling with a precision of about  $\Delta N_{\text{eff}} = \pm 0.26$  or better and thus will clearly decide if there is extra radiation in the universe [39]. If it finds convincing evidence for extra radiation, much in cosmology will have to be reconsidered besides our axion limits.

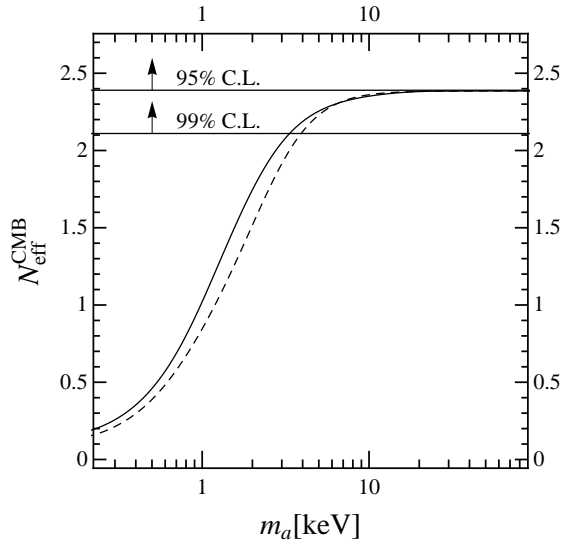


**Figure 6.** Radiation density during the CMB epoch ( $\delta = 1$ ). Solid and dashed lines are for hadronic and non-hadronic axions ( $C_e = 1/6$ ). The 95% and 99% C.L. lower limits from Eq. (5.2) are shown as horizontal lines.

## 5.2 Axion bounds

The cosmic energy density in neutrinos is modified by the factor  $(T_\nu^{\text{ax}}/T_\nu^{\text{std}})^4$  between the axion and standard cosmology. The results of Sec. 3 imply that this ratio can be expressed in terms of the quantity  $B_2$ , the modified  $(T/T_\nu)^3$  value after axions have disappeared

$$N_{\text{eff}} = 3 \left( \frac{11}{4B_2} \right)^{4/3}. \quad (5.3)$$

We show the variation with  $m_a$  for  $\delta = 1$  in Fig. 6. At sufficiently high  $m_a$ , the inverse decay process keeps thermal equilibrium during the decay. Even if axions decouple during  $e^+e^-$  annihilation they will re-thermalize with photons before decaying. In this case, we have an analytical expression

$$N_{\text{eff}} = 3 \left( \frac{11}{4} \frac{2(h_1 + 2)}{13} \frac{2}{3} \right)^{4/3} \left( \frac{3}{2 + h_1^{4/3}} \right). \quad (5.4)$$

For  $m_a > 20$  keV we have  $h_1 \simeq 1$  and  $N_{\text{eff}}$  reaches asymptotically the minimum neutrino dilution  $3(11/13)^{4/3} = 2.401$ . At much larger masses,  $m_a \sim \text{MeV}$ , axions would disappear in LTE before neutrino decoupling, leaving no trace in cosmology. Therefore, at  $m_a \sim \text{MeV}$  the value of  $N_{\text{eff}}$  shown in Fig. 6 reaches a plateau at the standard value  $N_{\text{eff}} = 3$ . Comparing with the cosmological limits of Eq. (5.2) we see that even the minimum neutrino dilution is only barely allowed at 95% C.L. and therefore disfavoured, but not credibly excluded.

For  $m_a \lesssim 20$  keV, axions decay increasingly out of equilibrium, creating entropy and reducing the final  $N_{\text{eff}}$  further. Comparing the calculated  $N_{\text{eff}}$  in Fig. 6 with the observational limits implies

$$m_a > 3 \text{ keV} \quad \text{at } 99\% \text{ C.L.} \quad (5.5)$$

The BBN limits reach to significantly larger masses, but the neutrino dilution limits are still nicely complementary.

## 6 CMB distortions

The primordial plasma is optically thick before recombination, yet the photons produced in axion decay can produce spectral distortions in the CMB, measured by the FIRAS experiment to follow a black-body spectrum with  $\mathcal{O}(10^{-4})$  precision [40].

After  $e^+e^-$  annihilation, photon thermal equilibrium is maintained by Compton scattering, double Compton scattering and bremsstrahlung. Compton scattering is the fastest of these processes, but it can only provide kinetic equilibrium while conserving the photon number density. Double Compton (DC) scattering and bremsstrahlung (BR) are slower but change photon number and thus achieve thermal equilibrium. After a redshift of approximately  $z \sim 3 \times 10^6$ , DC and BR no longer occur in equilibrium and any injection of photons leads to a non-zero pseudo degeneracy parameter,  $\mu$ . The FIRAS data restrict its value to

$$\mu < 9 \times 10^{-5}. \quad (6.1)$$

Therefore, even a minute fraction of axion decays occurring after this redshift leads to a measurable distortion.

Assuming that  $\mu$  is always small, we can cast its evolution as [41],

$$\frac{d\mu}{dt} = \frac{d\mu_a}{dt} - \mu \left( \frac{1}{t_{\text{DC}}} + \frac{1}{t_{\text{BR}}} \right), \quad (6.2)$$

where  $t_{\text{DC}}$  and  $t_{\text{BR}}$  are the  $\mu$  relaxation time scales due to the indicated processes (Appendix A) and  $d\mu_a/dt$  is the rate-of-change of  $\mu$  generated by Compton scattering from photon injection or disappearance resulting from axion decay or inverse decay. It is related to the change in photon energy  $d\rho_\gamma$  and photon number  $dn_\gamma$  by [41]

$$d\mu_a = \frac{1}{2.14} \left( \frac{3d\rho_\gamma}{\rho_\gamma} - 4\frac{dn_\gamma}{n_\gamma} \right), \quad (6.3)$$

assuming that  $\mu$  is small. To obtain our bounds we have implemented Eq. (6.2) in a numerical code describing the evolution of axion decay (Appendix A).

Our results are shown in Fig. 7, where we plot the final  $\mu$  value as a function of  $m_a$  and  $\delta$  for hadronic axions. In the left panel we fixed  $\delta = 1$ . In this case we find

$$m_a > 8.7 \text{ keV at } 95\% \text{ C.L.} \quad (6.4)$$

This bound is robust because  $\mu$  is a steep function of  $m_a$ . In particular it does not depend strongly on  $h_1$  and therefore is not expected to change significantly if we consider axions that couple to electrons, for which  $h_1$  will be slightly larger.

The CMB distortion effect depends sensitively on the axion-photon interaction strength for  $\delta < 1$  (right panel of Fig. 7). Generally the spectral distortions get larger for smaller  $\delta$  at a given  $m_a$ . For small  $\delta$ , the decay happens later, when the photon distribution is less protected against distortions.

For large  $\delta$  the final  $\mu$  changes sign from negative to positive with increasing  $m_a$  while for  $\delta < 0.1$   $\mu$  is always positive since axions decay non-relativistically injecting more energy than photon number. Of course, because of the sign change in  $\mu$  there exist some fine-tuned cases where the final  $\mu$  can be accidentally zero.

Finally, we note that for photon injection occurring below  $z \sim 10^5$  Compton scattering can no longer establish kinetic equilibrium, and the spectral distortion no longer takes the

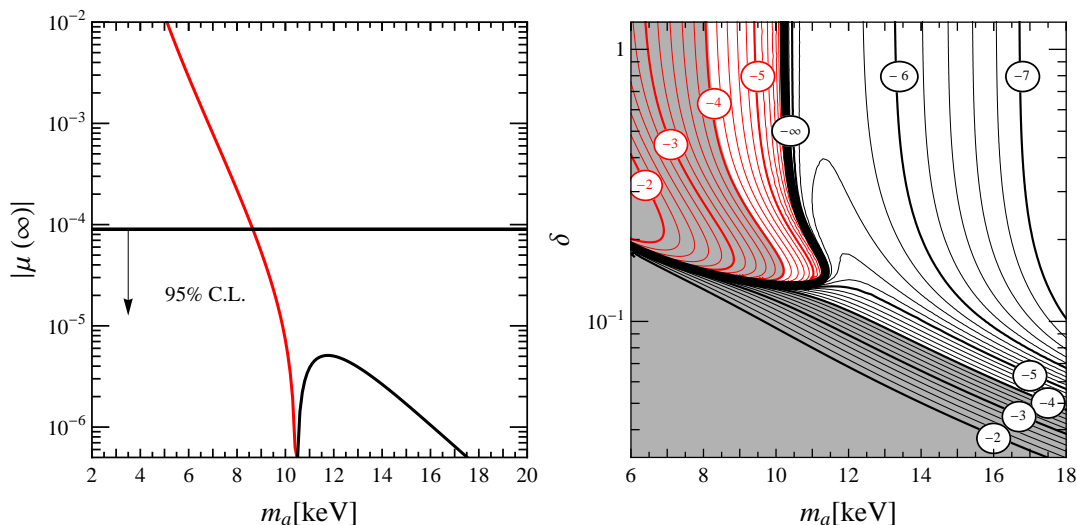


**Figure 7.** *Left:* Photon  $\mu$  parameter after axion decay ( $\delta = 1$ ). The observational upper bound is indicated. *Right:* Contours of  $\log_{10} |\mu|$  in the  $\delta$ - $m_a$ -plane where black/red corresponds to positive/negative values of  $\mu$  (The thick black line corresponds to the boundary  $\mu = 0$ ). The shaded area is excluded.

shape of a pseudo-degeneracy parameter. Rather, for  $10^3 < z < 10^5$  it can be represented by a Compton- $y$  parameter, and for  $z < 10^3$  the decay would show up as a bump in the infrared background. Most important for our purpose here is that the bound on  $\mu$  is weaker than on other spectral distortions and therefore our bound is robust even for  $m_a$  well below 1 keV.

## 7 Conclusions

Many cosmological particle-physics constraints were traditionally based on the idea that the successful predictions for the light-element abundances by BBN exclude additional radiation in the universe. However, over the past few years it has become apparent that both BBN and precision cosmology favour extra radiation on the level of around one effective neutrino family. While this preference is not yet strongly significant, it prevents one from deriving restrictive limits on possible additional forms of radiation.

We have studied a scenario where BBN still provides useful constraints on low-mass particles. Axions in the sub-MeV mass range would produce photons late enough to dilute baryons after BBN relative to photons. Therefore, the baryon abundance established at CMB decoupling by cosmological precision data is smaller than at BBN, leading to an unacceptably lowered deuterium abundance. We have shown that this argument requires the mass of axions to exceed around 300 keV. Additional arguments derive from the cosmic radiation content at CMB decoupling (neutrinos would be diluted relative to photons) and spectral CMB distortions. These bounds depend sensibly on the two-photon coupling, which determines the axion decay, rather than on the couplings to leptons and hadrons.

In the case of hadronic axions, together with the hot-dark matter limit, we thus find that cosmology alone excludes the  $m_a$  range 0.7 eV–300 keV. Our constraints are complementary to well-known stellar evolution limits and laboratory bounds, but based on completely different reasoning.

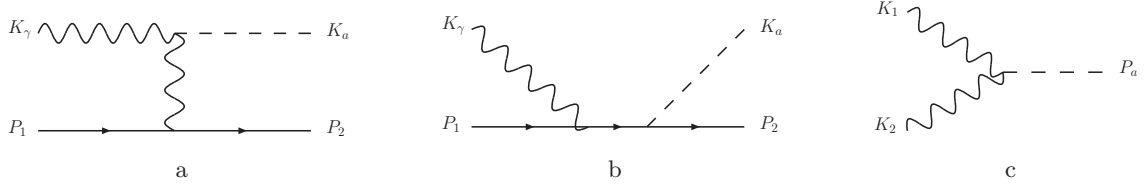


**Figure 8.** Primakoff (a) and Compton (b) processes on electrons and/or positrons and inverse two-photon decay (c). In the Compton case, there is also an  $u$ -channel diagram contributing.

## Acknowledgements

We acknowledge use of computing resources from the Danish Center for Scientific Computing (DCSC). In Munich, partial support by the Deutsche Forschungsgemeinschaft under the grant TR 27 “Neutrinos and beyond” and the Cluster of Excellence “Origin and Structure of the Universe” is acknowledged.

## A Axion out-of-equilibrium decay

### A.1 Boltzmann equation

We here compute the heating of the photon bath due to axion decay, with concomitant neutrino and baryon dilution and induced spectral  $\mu$  distortion of the CMB. The relevant axion interaction processes are Primakoff and Compton scattering on electrons and positrons and two-photon decay and its inverse (Fig. 8). The Boltzmann equation for the axion phase space density  $f_a(k_a, t)$  is

$$\frac{\partial f_a}{\partial t} - k_a H \frac{\partial f_a}{\partial k_a} = [C_e(k_a, f_a, T) + C_\gamma(k_a, f_a, T)] (f_a^{\text{eq}} - f_a), \quad (\text{A.1})$$

where  $H$  is the Hubble parameter. Here and in the following we denote boson four vectors as  $K = (\omega, \mathbf{k})$  and  $k = |\mathbf{k}|$ , whereas for fermions we use  $P = (E, \mathbf{p})$  and  $p = |\mathbf{p}|$ . Specifically we use  $\omega_a = (k_a^2 + m_a^2)^{1/2}$ . The collision integrals are

$$C_e = \frac{1}{2\omega_a} \int \frac{d^3\mathbf{p}_1}{(2\pi)^3 2E_1} \frac{d^3\mathbf{p}_2}{(2\pi)^3 2E_2} \frac{d^3\mathbf{k}_\gamma}{(2\pi)^3 2\omega_\gamma} (2\pi)^4 \delta^4(P_1 + K_\gamma - P_2 - K_a) |\mathcal{M}_e|^2 \\ \times f_1(E_1) f_\gamma(\omega_\gamma) [1 - f_2(E_2)] / f_a^{\text{eq}}(\omega_a), \quad (\text{A.2})$$

$$C_\gamma = \frac{1}{2\omega_a} \int \frac{d^3\mathbf{k}_1}{(2\pi)^3 2\omega_1} \frac{d^3\mathbf{k}_2}{(2\pi)^3 2\omega_2} (2\pi)^4 \delta^4(K_1 + K_2 - K_a) |\mathcal{M}_\gamma|^2 \\ \times [1 + f_1(\omega_1) + f_2(\omega_2)], \quad (\text{A.3})$$

where the particles are numbered as shown in Fig. 8. We assume thermal equilibrium between electrons and photons (temperature  $T$ ), neglecting possible chemical potentials (see below). Relevant thermal effects are an effective photon mass, preventing (inverse) decay at high  $T$  and screening effects for the Primakoff process. The spin- and polarization-summed squared

matrix elements are [42]

$$|\mathcal{M}_e|^2 = |\mathcal{M}_P|^2 + |\mathcal{M}_C|^2 + 2\text{Re}\{\mathcal{M}_P^* \mathcal{M}_C\}, \quad (\text{A.4})$$

$$|\mathcal{M}_P|^2 = \frac{4\pi\alpha g_{a\gamma}^2}{(t - m_\gamma^2)^2} \left\{ -2m_e^2 m_a^4 - t \left[ m_a^4 + 2(s - m_e^2)^2 - 2m_a^2(s + m_e^2) \right] \right. \\ \left. - 2t^2(s - m_a^2) - t^3 \right\}, \quad (\text{A.5})$$

$$|\mathcal{M}_C|^2 = 16\pi\alpha g_{ae}^2 \left\{ \frac{t^2 - m_a^2(3t - 4m_e^4)}{(s - m_e^2)(m_e^2 - u)} - m_a^2 \left( \frac{s + m_e^2}{(s - m_e^2)^2} + \frac{u + m_e^2}{(u - m_e^2)^2} \right) \right\}, \quad (\text{A.6})$$

$$2\text{Re}\{\mathcal{M}_P^* \mathcal{M}_C\} = -16\pi\alpha g_{ae} g_{a\gamma} \frac{(m_a^2 - t)^2}{(s - m_e^2)(m_\gamma^2 - t)}, \quad (\text{A.7})$$

$$|\mathcal{M}_\gamma|^2 = \frac{1}{2} g_{a\gamma}^2 m_a^2 (m_a^2 - 4m_\gamma^2), \quad (\text{A.8})$$

where we use the Mandelstam variables  $s = (P_1 + K_\gamma)^2$ ,  $t = (K_\gamma - K_a)^2$  and  $u = (K_a - P_1)^2$ . Also we have used  $g_{ae} = (C_e m_e)/f_a$ . We keep the photon mass only in the propagator to account for screening effects and on the external legs in (inverse) decay to retain a threshold. For inverse decays we find analytically

$$C_\gamma = \frac{m_a^2 - 4m_\gamma^2}{m_a^2} \frac{m_a}{\omega_a} \left[ 1 + \frac{2T}{p_a} \log \frac{1 - e^{-(\omega_a + p_a)/2T}}{1 - e^{-(\omega_a - p_a)/2T}} \right] \Gamma_{a \rightarrow \gamma\gamma}. \quad (\text{A.9})$$

The Primakoff and Compton terms are much more complicated and have to be handled numerically. In this case it is much simpler to compute axion decoupling directly based on the Boltzmann equation for the axion number density, cf. Eq. (3.5). Integrating Eq. (A.1) over the axion phase space and defining  $Y_a = n_a/s$  (total entropy  $s$ ) we find

$$s \frac{dY_a}{dt} = \int \frac{d^3\mathbf{k}_a}{(2\pi)^3} (C_e + C_\gamma) (f_a - f_a^{\text{eq}}) \equiv (\Gamma_e + \Gamma_\gamma)(n_a - n_a^{\text{eq}}), \quad (\text{A.10})$$

where we have used comoving entropy conservation,  $d(sR^3)/dt = 0$ , and assumed that  $f_a$  is proportional to  $f_a^{\text{eq}}$ , a reasonable approximation for computing the decoupling of a relativistic species. The second equality defines the rates we have used in Sec. 3. Entropy conservation can also be used to obtain the temperature-time relation that allows us to use the former as the independent variable

$$\frac{d}{dt} = -H \left( \frac{d \log s}{d \log T^3} \right)^{-1} \frac{d}{d \log T}. \quad (\text{A.11})$$

which, together with Eq. (A.10), leads to Eq. (3.5).

Our bounds do not depend on a precise determination of  $h_1$ , the axion abundance after the  $e^\pm$  annihilation epoch, so we have solved Eq. (3.5) under two simplifying approximations. First, we note that the axion contribution to  $s$  is relatively small (the contribution from photons and neutrinos are at least a factor 4.4 bigger) so we can neglect it in  $s$  and in its derivative. Second, we have assumed Maxwell-Boltzmann distributions for all particles to find the average Primakoff/Compton rate, whereas decay and inverse decay are tractable without this simplification<sup>2</sup>. It is then easy to obtain numerically the evolution of  $Y_a$  and the value of  $h_1$  at  $T_1 = m_e/10$ .

<sup>2</sup> We have checked that our results do not differ significantly with the full results derived in [43, 44] for the relativistic limit  $T \gg m_e, m_a$ .



## A.2 Axion decay

At  $T \sim m_e/10$  essentially all the  $e^+e^-$  entropy has been transferred to photons and axions. The  $e^+e^-$  number density is exponentially suppressed, so we can ignore Primakoff and Compton. To compute numerically the photon heating when axions finally decay we evolve the axion phase-space distribution. The initial condition is set at  $T = m_e/10$  by computing the axion temperature that gives  $n_a = h_1 n_a^{\text{eq}}$  when assuming  $f_a$  to be a thermal distribution, albeit at a different temperature than photons. Note that the Boltzmann equation (A.1) can be much simplified by considering comoving momentum  $\tilde{k}_a \equiv k_a(R/R_0)$ , where  $R_0$  is a reference scale factor. Defining  $g_a(\tilde{k}_a, t) \equiv f(k_a, t)$ , the l.h.s. of Eq. (A.1) simply is  $dg_a/dt$  and the Boltzmann equation describing the decay becomes

$$\frac{dg_a}{dt} = -(g_a - g_a^{\text{eq}}) C_\gamma, \quad (\text{A.12})$$

with  $C_\gamma$  given by Eq. (A.9).

We next compute the energy transfer to photons. The Boltzmann equation for the photon phase space distribution  $f_\gamma(k_\gamma, t)$  can be written as

$$\begin{aligned} \frac{\partial f}{\partial t} - k_\gamma H f = & \frac{1}{2\omega_\gamma} \int \frac{d^3 \mathbf{k}_a}{(2\pi)^3 2\omega_a} \frac{d^3 k'_\gamma}{(2\pi)^3 2\omega'_\gamma} (2\pi)^4 \delta^4(K_a - K_\gamma - K'_\gamma) |\mathcal{M}_\gamma|^2 \\ & \times [1 + f_\gamma(\omega_\gamma) + f_\gamma(\omega'_\gamma)] (f_a^{\text{eq}} - f_a) \\ & + \text{interaction terms with relic baryons and electrons.} \end{aligned} \quad (\text{A.13})$$

The assumption that photons are always in kinetic equilibrium during axion decay is equivalent to saying that the two sources on the r.h.s. will readjust themselves such that  $f_\gamma$  is always of Bose-Einstein form. The evolution of the small photon chemical potential is considered below and neglected in the axion decay calculation.

Multiplying by the photon energy  $\omega_\gamma$  and integrating over phase space we obtain the equation for the evolution of the photon energy density

$$\frac{\partial \rho_\gamma}{\partial t} - 4H\rho_\gamma = \int \frac{d^3 k_a}{(2\pi)^3} C_\gamma (g_a - g_a^{\text{eq}}) \omega_\gamma. \quad (\text{A.14})$$

It states that the energy gain or loss of photons is due to axion decays or inverse decays. We have neglected the terms involving baryons and electrons. The evolution of the photon number density can be obtained analogously, but one has to take into account that double Compton and bremsstrahlung can yet modify the photon number (see below).

To proceed further we define suitable time coordinates. As stated in the main text, neutrino temperature  $T_\nu$  provides a natural reference to write the photon temperature in terms of  $T_\nu$  through the parameter  $B$  that was defined in Eq. (3.6). Introducing the variables  $x = m_a/T_\nu$  and  $y = P/T_\nu$  we have

$$\frac{d}{dt} = xH \frac{d}{dx}, \quad (\text{A.15})$$

with  $H$  defined in Eq. (3.3). The evolution of  $g_a$  in Eq. (A.12) is in final form

$$\frac{dg_a}{dx} = \frac{C_\gamma}{xH} (g_a - g_a^{\text{eq}}). \quad (\text{A.16})$$

Furthermore, the comoving photon energy density  $\rho_\gamma R^4 = \pi^2 (TR)^4/15$  can be expressed in terms of  $B^4$ . After some substitutions we find

$$\frac{dB^4}{dx} = -\frac{15}{\pi^2} \int \frac{y^2 dy}{2\pi^2} \frac{C_\gamma}{H} \frac{\sqrt{x^2 + y^2}}{x} (g_a - g_a^{\text{eq}}). \quad (\text{A.17})$$

So far we have ignored the effects of the photon chemical potential. As explained in Sec. 6 the evolution of a small  $\mu$  is given by Eq. (6.2). The characteristic time scales for double Compton scattering and bremsstrahlung to erase  $\mu$  are given in Ref. [41]. Translated to our notation they are

$$t_{\text{DC}} = 2.1 \times 10^{33} \text{ s } (1 - Y_p/2)^{-1} (\Omega_b h^2)^{-1} \left( \frac{x T_{\gamma, \text{today}}}{m_a} \right)^{9/2} \frac{B_{\text{today}}^3}{B^{3/2}} \frac{1}{B_1^6}, \quad (\text{A.18})$$

$$t_{\text{BR}} = 3.4 \times 10^{25} \text{ s } (1 - Y_p/2)^{-1} (\Omega_b h^2)^{-3/2} \left( \frac{x T_{\gamma, \text{today}}}{m_a} \right)^{13/4} \frac{B_{\text{today}}^{9/2}}{B^{-5/4}} \frac{1}{B_1^{27/4}},$$

with  $Y_p$  the helium mass fraction and  $\Omega_b h^2$  the baryon density normalized to the critical density today (here  $h$  stands for the usual dimensionless Hubble constant). We use the values  $Y_p = 0.23$ ,  $T_{\gamma, \text{today}} = 2.725 \text{ K}$  and  $\Omega_b h^2 = 0.0223$ . Using Eq. (A.14) and its counterpart for photon number, only retaining the axion decay induced  $dn_\gamma$ , the injection can be written as a time-dependent source for the pseudo degeneracy parameter

$$\frac{d\mu_a}{dx} = \frac{1}{2.14} \int \frac{dy y^2}{2\pi^2} (g_a - g_a^{\text{eq}}) \frac{C_\gamma}{H} \frac{\sqrt{x^2 + y^2}}{x} \left( \frac{45}{\pi^2 B^4} - \frac{8\pi^2}{\zeta(3) B^3 \sqrt{x^2 + y^2}} \right). \quad (\text{A.19})$$

We have numerically solved the evolution equations for the axion phase space distribution Eq. (A.16), the photon temperature Eq. (A.17), and the pseudo degeneracy parameter Eq. (6.2), together with the initial conditions  $\mu_0 = 0$  and for  $B_1$  given by Eq. (3.8) as a function of  $h_1$ . The latter was computed before, cf. Fig. (2). Note that the expressions for  $t_{\text{DC}}$  and  $t_{\text{BR}}$ , cf. Eq. (A.18), require the value of  $B_{\text{today}}$ , so in order to compute the chemical potential we first compute the evolution of  $B$  and determine  $B_{\text{today}}$  and then run again the evolution to compute the final value of  $\mu$ .

## References

- [1] J. Lesgourgues and S. Pastor, “Massive neutrinos and cosmology”, Phys. Rept. **429** (2006) 307 [astro-ph/0603494].
- [2] S. Hannestad, H. Tu and Y. Y. Y. Wong, “Measuring neutrino masses and dark energy with weak lensing tomography”, JCAP **0606** (2006) 025 [astro-ph/0603019].
- [3] S. Hannestad and G. G. Raffelt, “Cosmological mass limits on neutrinos, axions, and other light particles”, JCAP **0404** (2004) 008 [hep-ph/0312154].
- [4] S. Hannestad, A. Mirizzi and G. G. Raffelt, “New cosmological mass limit on thermal relic axions”, JCAP **0507** (2005) 002 [hep-ph/0504059].
- [5] A. Melchiorri, O. Mena and A. Slosar, “An improved cosmological bound on the thermal axion mass”, Phys. Rev. D **76** (2007) 041303 [arXiv:0705.2695].
- [6] S. Hannestad, A. Mirizzi, G. G. Raffelt and Y. Y. Y. Wong, “Cosmological constraints on neutrino plus axion hot dark matter”, JCAP **0708** (2007) 015 [arXiv:0706.4198].

- [7] S. Hannestad, A. Mirizzi, G. G. Raffelt and Y. Y. Y. Wong, “Cosmological constraints on neutrino plus axion hot dark matter: Update after WMAP-5”, JCAP **0804** (2008) 019 [arXiv:0803.1585]
- [8] S. Hannestad, A. Mirizzi, G. G. Raffelt and Y. Y. Y. Wong, “Neutrino and axion hot dark matter bounds after WMAP-7”, JCAP **1008** (2010) 001 [arXiv:1004.0695].
- [9] P. Sikivie, “Axion cosmology”, Lect. Notes Phys. **741** (2008) 19 [astro-ph/0610440].
- [10] G. G. Raffelt, “Astrophysical axion bounds”, Lect. Notes Phys. **741** (2008) 51 [hep-ph/0611350].
- [11] E. Arik *et al.* (CAST Collaboration), “Probing eV-scale axions with CAST”, JCAP **0902** (2009) 008 [arXiv:0810.4482].
- [12] Y. Inoue, Y. Akimoto, R. Ohta, T. Mizumoto, A. Yamamoto and M. Minowa, “Search for solar axions with mass around 1 eV using coherent conversion of axions into photons”, Phys. Lett. B **668** (2008) 93 [arXiv:0806.2230].
- [13] E. Massó and R. Toldrà, “On a light spinless particle coupled to photons”, Phys. Rev. D **52** (1995) 1755 [hep-ph/9503293].
- [14] E. Massó and R. Toldrà, “New constraints on a light spinless particle coupled to photons”, Phys. Rev. D **55** (1997) 7967 [hep-ph/9702275].
- [15] E. Aver, K. A. Olive and E. D. Skillman, “A new approach to systematic uncertainties and self-consistency in helium abundance determinations”, JCAP **1005**, 003 (2010) [arXiv:1001.5218].
- [16] Y. I. Izotov and T. X. Thuan, “The primordial abundance of 4He: evidence for non-standard big bang nucleosynthesis”, Astrophys. J. **710**, L67 (2010) [arXiv:1001.4440].
- [17] J. Hamann, S. Hannestad, G. G. Raffelt and Y. Y. Y. Wong, “Observational bounds on the cosmic radiation density”, JCAP **0708** (2007) 021 [arXiv:0705.0440].
- [18] J. Hamann, S. Hannestad, J. Lesgourgues, C. Rampf and Y. Y. Y. Wong, “Cosmological parameters from large scale structure—geometric versus shape information”, JCAP **1007** (2010) 022 [arXiv:1003.3999].
- [19] E. Komatsu *et al.*, “Seven-Year Wilkinson Microwave Anisotropy Probe (WMAP) observations: Cosmological interpretation”, arXiv:1001.4538.
- [20] M. C. Gonzalez-Garcia, M. Maltoni and J. Salvado, “Robust cosmological bounds on neutrinos and their combination with oscillation results”, JHEP **1008** (2010) 117 [arXiv:1006.3795].
- [21] J. Hamann, S. Hannestad, G. G. Raffelt, I. Tamborra and Y. Y. Y. Wong, “Cosmology favoring extra radiation and sub-eV mass sterile neutrinos as an option”, Phys. Rev. Lett. **105** (2010) 181301 [arXiv:1006.5276].
- [22] F. Bergsma *et al.* [CHARM Collaboration], “Search for axion like particle production in 400-GeV proton - copper interactions”, Phys. Lett. B **157** (1985) 458.
- [23] A. Konaka *et al.*, “Search for neutral particles in electron beam dump experiment”, Phys. Rev. Lett. **57** (1986) 659.
- [24] E. M. Riordan *et al.*, “A search for short lived axions in an electron beam dump experiment”, Phys. Rev. Lett. **59** (1987) 755.
- [25] A. Bross *et al.*, “A search for shortlived particles produced in an electron beam dump”, Phys. Rev. Lett. **67** (1991) 2942-2945.
- [26] M. Altmann *et al.*, “Search for the electron positron decay of axions and axion - like particles at a nuclear power reactor at Bugey”, Z. Phys. **C68** (1995) 221-227.
- [27] H. M. Chang *et al.* [ TEXONO Collaboration ], Phys. Rev. **D75** (2007) 052004.

- [hep-ex/0609001].
- [28] R. D. Peccei, “The strong CP problem and axions”, *Lect. Notes Phys.* **741** (2008) 3 [hep-ph/0607268].
  - [29] K. Nakamura (Particle Data Group), “Review of particle physics”, *J. Phys. G* **37** (2010) 075021.
  - [30] J. E. Kim, “Weak interaction singlet and strong CP invariance”, *Phys. Rev. Lett.* **43** (1979) 103.
  - [31] M. A. Shifman, A. I. Vainshtein and V. I. Zakharov, “Can confinement ensure natural CP invariance of strong interactions?”, *Nucl. Phys. B* **166** (1980) 493.
  - [32] A. R. Zhitnitsky, “On possible suppression of the axion hadron interactions,” (In Russian) *Sov. J. Nucl. Phys.* **31** (1980) 260.
  - [33] M. Dine, W. Fischler and M. Srednicki, “A simple solution to the strong CP problem with a harmless axion”, *Phys. Lett.* **B104** (1981) 199.
  - [34] G. B. Gelmini, S. Nussinov and T. Yanagida, “Does nature like Nambu-Goldstone bosons?”, *Nucl. Phys.* **B219** (1983) 31.
  - [35] E. W. Kolb and M. S. Turner, “The early universe”, *Front. Phys.* **69** (1990) 1-547.
  - [36] O. Pisanti, A. Cirillo, S. Esposito, F. Iocco, G. Mangano, G. Miele and P. D. Serpico, “PARthENoPE: Public Algorithm Evaluating the Nucleosynthesis of Primordial Elements”, *Comput. Phys. Commun.* **178** (2008) 956 [arXiv:0705.0290].
  - [37] M. Pettini, B. J. Zych, M. T. Murphy, A. Lewis and C. C. Steidel, “Deuterium Abundance in the Most Metal-Poor Damped Lyman alpha System: Converging on  $\Omega_b$ ,” *Mon. Not. R. Astron. Soc.* **391** (2008) 14991510 [arXiv:0805.0594].
  - [38] G. Mangano, G. Miele, S. Pastor, T. Pinto, O. Pisanti and P. D. Serpico, “Relic neutrino decoupling including flavour oscillations”, *Nucl. Phys. B* **729** (2005) 221 [hep-ph/0506164].
  - [39] J. Hamann, J. Lesgourgues and G. Mangano, “Using BBN in cosmological parameter extraction from CMB: a forecast for Planck”, *JCAP* **0803** (2008) 004 [arXiv:0712.2826].
  - [40] D. J. Fixsen, E. S. Cheng, J. M. Gales, J. C. Mather, R. A. Shafer and E. L. Wright, “The cosmic microwave background spectrum from the full COBE/FIRAS data set”, *Astrophys. J.* **473** (1996) 576 [astro-ph/9605054].
  - [41] W. Hu and J. Silk, “Thermalization and spectral distortions of the cosmic background radiation”, *Phys. Rev. D* **48** (1993) 485.
  - [42] S. J. Brodsky, E. Mottola, I. J. Muzinich and M. Soldate, “Laser induced axion photoproduction”, *Phys. Rev. Lett.* **56** (1986) 1763.
  - [43] E. Braaten and T. C. Yuan, “Calculation of screening in a hot plasma,” *Phys. Rev. Lett.* **66** (1991) 2183-2186.
  - [44] M. Bolz, A. Brandenburg and W. Büchmüller, “Thermal production of gravitinos,” *Nucl. Phys.* **B606** (2001) 518-544.